# Tunneling Anisotropic Magnetoresistance: A Spin-Valve-Like Tunnel Magnetoresistance Using a Single Magnetic Layer

C. Gould,[1] C. Rüster,[1] T. Jungwirth,[2,3,4] E. Girgis,[1] G. M. Schott,[1] R. Giraud,[1] K. Brunner,[1] G. Schmidt,[1] and L. W. Molenkamp[1]

[1]*Physikalisches Institut (EP3), Universität Würzburg, Am Hubland, D-97074 Würzburg, Germany*
[2]*Institute of Physics ASCR, Cukrovarnická 10, 162 53 Praha 6, Czech Republic*
[3]*School of Physics and Astronomy, University of Nottingham, Nottingham NG7 2RD, United Kingdom*
[4]*Department of Physics, University of Texas, Austin, Texas 78712-0264, USA*

(Received 25 May 2004; published 9 September 2004)

We introduce a new class of spintronic devices in which a spin-valve-like effect results from strong spin-orbit coupling in a single ferromagnetic layer rather than from injection and detection of a spin-polarized current by two coupled ferromagnets. The effect is observed in a normal-metal–insulator–ferromagnetic-semiconductor tunneling device. This behavior is caused by the interplay of the anisotropic density of states in (Ga,Mn)As with respect to the magnetization direction and the two-step magnetization reversal process in this material.

DOI: 10.1103/PhysRevLett.93.117203 PACS numbers: 85.75.Mm, 75.50.Pp

Devices relying on spin manipulation are hoped to provide low-dissipative alternatives for microelectronics. Furthermore, spintronics is expected to lead to full integration of information processing and storage functionalities, opening attractive prospects for the realization of instant on-and-off computers. A primary goal of current spintronics research is to realize a device with metal spin-valve-like behavior [1] in an all semiconductor-based structure enhancing integration of spintronics with existing microelectronics technologies. An oft proposed scheme for such a device consists of a tunnel barrier between two ferromagnetic semiconductors. As such, (Ga, Mn)As/(Al, Ga)As/(Ga, Mn)As structures have previously been studied [2,3] with some promising results. However, realizing the full potential of these systems will require a complete understanding of the physics of tunneling into (Ga,Mn)As, which we have found to be rather different than previously thought.

In this spirit, we investigate transport in a structure consisting of a single ferromagnetic (Ga,Mn)As layer fitted with a tunnel barrier and a nonmagnetic metal contact. We report some of the rich experimental properties of such a tunneling structure and provide an interpretation of the measured spin-valve-like effect as a tunneling anisotropic magnetoresistance (TAMR) due to a two-step magnetization reversal and a magnetization dependent density of states (DOS) in the (Ga,Mn)As layer.

The magnetic layer in our sample is a 70 nm thick epitaxial (Ga,Mn)As film grown by low temperature (270 °C) molecular beam epitaxy onto a GaAs (001) substrate [4]. High-resolution x-ray diffraction showed that the sample had high crystalline quality comparable to that of the substrate. From the measured lattice constant and the calibration curves of Ref. [5], the Mn concentration in the ferromagnetic layer is roughly 6%. Etch capacitance-voltage control measurements yielded a hole density estimate of $\sim 10^{21}$ cm$^{-3}$ and the Curie temperature of 70 K was determined from SQUID measurements.

After growth, the sample surface was Ar sputtered to remove any potential oxides, and a 1.4 nm Al layer was deposited at a rate of 0.4 Å/ sec and a base pressure of $2 \times 10^{-6}$ mbar using Ar gas. The Al layer was oxidized *in situ* using 100 mbar of pure oxygen for 8 h, producing a closed AlOx layer and thereby forming a tunnel barrier. An electrical contact was then fashioned onto the structure by evaporating 5 nm of Ti as a sticking layer followed by 300 nm of Au. Standard optical lithography and chemically assisted ion beam etching were then used to pattern the device as shown in Fig. 1(a). In the first step, material is etched away, leaving only the central $100 \times 100$ $\mu$m$^2$ square pillar consisting of the metal contact on a tunnel barrier. The surrounding tungsten sticking layer and Au contact are then deposited onto the (Ga,Mn)As surface, providing a back contact.

The (Ga,Mn)As resistivity is $1.1 \times 10^{-3}$ $\Omega$ cm, typical for high quality material [6]. This corresponds to a resistance of $\sim 10$ $\Omega$ between the central pillar and the backside contact. This was confirmed by measuring the resistance through similar pillars without a tunnel barrier. This resistance is over 2 orders of magnitude lower than that of the total device, rendering any bulk magnetoresistance of the (Ga,Mn)As negligible.

The sample was inserted into a magnetocryostat allowing for the application of magnetic fields of up to 300 mT in any direction. Results discussed here are for fields in the plane of the magnetic layer with the field direction given by its angle $\phi$ with respect to the [100] direction, as indicated in Fig. 1(a).

Figure 1(b) presents representative magnetoresistance curves at various angles. For each curve, the field is swept from negative saturation to positive saturation and back, but the plot focuses on the interesting region

  

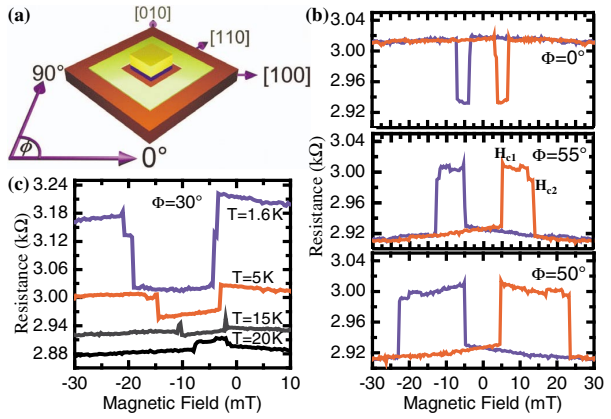


FIG. 1 (color online). (a) Device schematic showing the contact geometry and the crystallographic directions. (b) Hysteretic magnetoresistance curves acquired at 4.2 K with 1 mV bias by sweeping the magnetic field along the 0°, 50°, and 55° directions. Spin-valve-like features of varying widths and signs are clearly visible, delimited by two switching events labeled $H_{c1}$ and $H_{c2}$. The magnetoresistance is independent of the bias direction or amplitudes up to 1 meV. (c) TAMR along 30° for temperatures from 1.6 to 20 K, showing a change of sign of the signal. The curves are vertically offset for clarity.

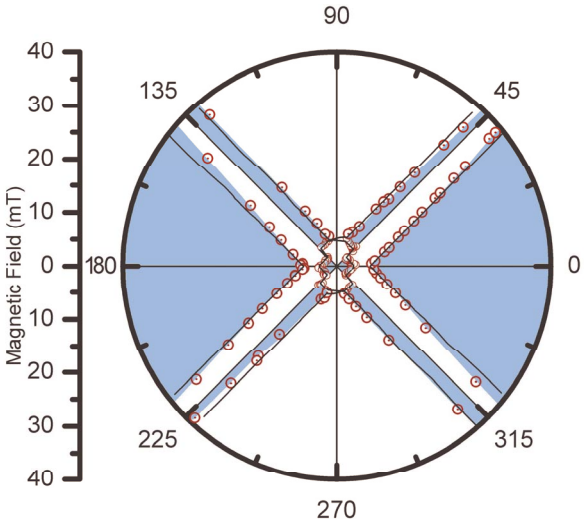


FIG. 2 (color online). Polar plot compiled from individual magnetoresistance curves. The circles indicate the switching events $H_{c1}$ and $H_{c2}$ from the individual curves. The shaded areas are regions where the sample is in a high-resistance state. The solid lines are a fit to the model described in the text.

from −30 to +30 mT. In all cases, the magnetoresistance shows spin-valve-like behavior with an amplitude of ∼3% delimited by two switching events ( labeled $H_{c1}$ and $H_{c2}$ in the figure) between which the resistance of the sample is different from its value outside these events. However, the width and even the sign of the TAMR feature depend on $\phi$. In comparing the curves of Fig. 1(b), we emphasize that, despite the feature changing signs as a function of $\phi$, the device appears to have only two distinct resistance states: a low one of ∼2920 Ω and a high one of ∼3000 Ω.

In order to better understand this behavior, we summarize the data from field sweeps at many angles in the polar plot of Fig. 2. Here the open circles represent the fields at which the switching events $H_{c1}$ and $H_{c2}$ occur in the individual sweeps. These delimit boundaries between sections of higher and lower resistance. Shaded areas indicate regions where the sample is in its high-resistance state. Viewed in this way, the loci of switching events form a highly symmetric pattern with a striking resemblance to switching previously observed in magneto-optical studies of epitaxial Fe films [7] and (Ga,Mn)As [8], as well as in transport studies on (Ga,Mn)As in the in-plane Hall geometry [9], and associated with materials that reverse their magnetization $M$ in two steps by the nucleation and propagation of 90° domain walls.

Within single-domain theory, the expression for the total magnetic energy $E_m$ of our system is

$$E_m = K_u \sin^2(\theta) + K_c \sin^2(2\theta) - MH\cos(\theta - \phi), \quad (1)$$

where $K_c$ is the cubic anisotropy known to be dominant in (Ga,Mn)As [8–10], while $K_u$ is the uniaxial anisotropy which is also often observed in (Ga,Mn)As [8]. $H$ is the amplitude of the applied magnetic field and $\theta$ is the angle of the magnetization measured from the [100] crystal direction.

Since the magnetization reversal takes place through domain walls propagating through the structure, the picture of Stoner–Wohlfarth [11] of a coherent magnetization reversal does not apply (neglecting rotations away from the cubic easy axis at higher $H$). Instead, as discussed in Ref. [7], the magnetization will switch from its local minimum to the global energy minimum as long as the energy gained in doing so is larger than the energy required to nucleate or propagate a domain wall through the sample. Calling this energy $\epsilon$, it follows from the form of $E_m$ that as $H$ is swept the switching of the magnetization can take place in two steps. In the first step, $M$ switches from the cubic easy axis closest to the initial direction of $H$ to a global easy axis 90° askew from this one. Then, in the second step, $M$ switches by an additional 90° completing its reversal. Pursuing the analysis, one finds that the fields at which these switching events take place are given by $H_{c1,2} = (\epsilon \pm K_u)/[M||\cos(\phi)| \pm |\sin(\phi)||]$, where the plus (minus) sign in the denominator is for $H_{c1}$ ($H_{c2}$). The sign before $K_u$ depends on if the switching is towards or away from a uniaxial easy axis. The sign therefore reverses every 90° and is opposite for $H_{c1}$ and $H_{c2}$ [7]. Fitting the above equation to our data produces the solid line in the polar plot of Fig. 2. This yields a value of 450 erg/cm$^3$ for $K_u$ and 1550 erg/cm$^3$ for $\epsilon$. We confirmed the two-step switching behavior of the sample through SQUID measurements.

From this analysis and Fig. 2 it is clear that our sample is in a high-resistance state when $M$ lies along the [100] or

$[\bar{1}00]$ crystallographic direction, and has a lower resistance when $M$ is along [010] or $[0\bar{1}0]$. This picture is further supported by the behavior of the magnetoresistance at higher $H$. When the magnetic field is not aligned along an easy axis, and the field is swept to full saturation, the magnetization will rotate away from the easy axis to the direction parallel to the field. A corresponding gradual change in resistance is then observed consistent with a cubic anisotropy at least an order of magnitude larger than $K_u$, in agreement with Ref. [9].

We now turn to a theoretical analysis illustrating that anisotropies in the (Ga,Mn)As DOS with respect to the magnetization orientation are large enough to explain the observation of the TAMR effect. The electronic structure of the (Ga,Mn)As is calculated using the $\vec{k} \cdot \vec{p}$ envelope function description of the GaAs host valence bands in the presence of an effective exchange field, $\vec{h} = J_{pd}\vec{S}_{\mathrm{Mn}}$, produced by the polarized Mn local moments with spin density $\vec{S}_{\mathrm{Mn}}$ [12]. The broken in-plane cubic symmetry responsible for the difference between tunnel resistances for $M$ along [100] and [010] is theoretically modeled by introducing an in-plane uniaxial strain of order 0.1%. Because of a very strong spin-orbit interaction in the valence band, such a small strain leads to values of $K_u$ comparable to the one estimated above and also to sizable DOS anisotropies.

Defining the partial DOS as the DOS at a given $k_z$ and for a given band, we show in Fig. 3 the relative partial DOS anisotropy $[\Delta\mathrm{DOS}_{\mathrm{partial}} \equiv \mathrm{DOS}_{\mathrm{partial}}(M \| [010]) - \mathrm{DOS}_{\mathrm{partial}}(M \| [100])]$ at the Fermi energy $E_F$ calculated as a function of the out-of-plane wave vector $k_z$ for each of the four occupied bands that derive from the GaAs heavy- and light-hole states which are spin-split due to

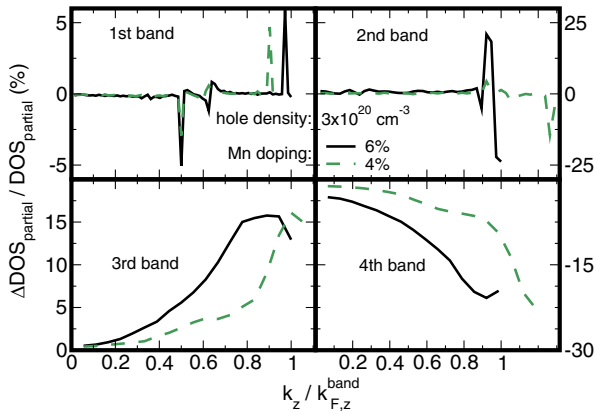


FIG. 3 (color online). The relative difference between partial DOS at the Fermi energy for $M$ along [010] and[100] directions is plotted separately for each of the four occupied valence bands. Note that in the ferromagnetic state, even the near $k = 0$ states, cannot properly be called light and heavy holes due to the $pd$ exchange interaction. Dashed lines correspond to $\mathrm{Mn_{Ga}}$ concentration of 4%; solid lines corresponding to 6% Mn doping are shown for comparison.

the presence of the Mn-moment induced exchange field [12]. $k_{F,z}^{\mathrm{band}}$ is the Fermi wave vector in the given band for $\mathrm{Mn_{Ga}}$ concentration of 6%.

Note that the experimental Curie temperature of 70 K is reproduced theoretically assuming the hole density $3 \times 10^{20}$ cm$^{-3}$ and 4% of the cation sites occupied by Mn, which is reasonably consistent with the experimental estimates. The total DOS ($\mathrm{DOS_{total}}$) obtained by integrating over all $k_z$ up to the Fermi wave vector $k_{F,z}$ and summing over all bands, has an anisotropy at $E_F$ of less than 1% with respect to the magnetization orientation. The tunnel conductance is, however, proportional to the $\mathrm{DOS_{total}}$ only if in-plane momentum is not conserved during the tunneling. For cleaner barriers and interfaces, in-plane momentum is at least partially conserved resulting in, roughly speaking, a higher probability of tunneling for states with higher band and $k_z$ indices. As demonstrated in Fig. 3, the $\mathrm{DOS_{partial}}$ of these states can change by tens of percents upon magnetization reorientation. Figure 3 also suggests that the magnitude and even the sign of the overall tunnel magnetoresistance effect depend on parameters of the (Ga,Mn)As film, such as the density of local spins on substitutional Mn impurities, or on the barrier and interface character which may select different ranges of band and $k_z$ states that dominate the tunneling current.

To estimate the overall size of the magnetoresistance effect produced by the (Ga,Mn)As $\mathrm{DOS_{partial}}$ anisotropy, we start with the assumption that for clean barriers (perfect in-plane momentum conservation) the tunneling is dominated by states in (Ga,Mn)As with $k_z$ close to $k_F$ in each band and that the tunneling probability of these states is independent of the band index. We then gradually relax the momentum conservation condition by adding states at $E_F$ with decreasing $k_z$. In Fig. 4 we plot the relative difference between this integrated $\mathrm{DOS_{int}}$ (integrated over the assumed range of $k_z$ contributing to tunneling and summed over the four occupied bands) for the two magnetization orientations. For $\sim$10% of the total DOS at $E_F$ participating in the tunneling, the theoretical $\mathrm{DOS_{int}}$ anisotropy is consistent with the experimentally observed TAMR of order several percent.

The curves in the left panel of Fig. 4 are labeled by different Mn doping concentrations and illustrate the general dependence of the magnetoresistance effect on the Mn local spin density. On a mean-field level this can be understood by recalling that the (Ga,Mn)As electronic structure depends only on the overall value of the effective exchange field $\vec{h} = J_{pd}\vec{S}_{\mathrm{Mn}}$, whether the spin-density magnitude $|S_{\mathrm{Mn}}|$ changes through varying the number of Mn impurities at a fixed temperature or through the temperature-dependent average spin polarization of an individual Mn local moment at a fixed doping level. The data in the left panel of Fig. 4 therefore suggest that the sign of the TAMR can change with temperature. We

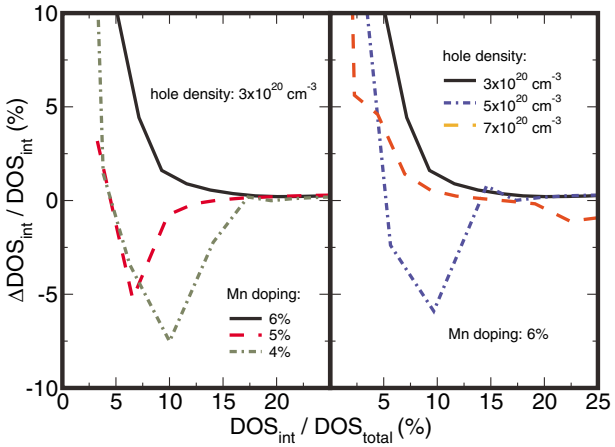


FIG. 4 (color online). The relative integrated DOS anisotropy is plotted for different Mn (left panel) and hole (right panel) concentrations. The $x$ axis represents the DOS at the Fermi energy that is assumed to contribute to tunneling, relative to the total DOS at the Fermi energy. Moving from left to right corresponds to gradually relaxing the momentum conservation condition.

emphasize that this change in sign occurs without a change in sign of the uniaxial anisotropy energy constant. The right panel in Fig. 4 also predicts a strong dependence of the TAMR on the number of holes in the (Ga,Mn)As valence band.

In our sample the Mn doping and hole density are obviously fixed. The temperature dependence, however, can be tested and the experiment confirms the change of sign seen in the above theoretical curves. Figure 1(c) shows a set of magnetoresistance curves along 30° for temperatures from 1.6 to 20 K. At 1.6 K, the TAMR signal is negative. Its amplitude gradually decreases to zero by 15 K, changes sign, and grows again as temperature is raised to 20 K. In fact, as temperature is increased from 4 to 20 K, the entire polar plot reverses signs. Finally, the TAMR disappears by 30 K, when the magnetic anisotropy energy is no longer resolvable. Since the sign of $K_u$ does not change with temperature, this is an experimental confirmation that the transport and magnetic anisotropies can vary independently in our system.

The TAMR studied here shows a rich phenomenology that opens new directions in spintronics research. Avoiding the second ferromagnetic layer may have fundamental consequences for the operation at high temperatures as it eliminates the need for a buried ferromagnetic layer which cannot be effectively treated by post-growth annealing [13]. The data also demonstrate that the sign of the spin-valve-like signal, i.e., whether a high- or low-resistance state is realized at saturation, can change with the angle at which magnetic field is applied, with temperature, or with structural parameters of the (Ga,Mn)As layer, interfaces, and the tunnel barrier.

Last but not least, our experiments provide a new perspective on tunnel magnetoresistance in structures with two ferromagnetic contacts. We demonstrate the need for caution in analyzing spin-valve experiments, especially in materials where strong spin-orbit coupling is present. As we have seen here, the existence of a spin-valve-like signal does not automatically imply the injection and detection of a spin-polarized current in the tunneling structure. Instead, two distinct material properties combined in a constructive way can lead to bistable magnetoresistive devices with unprecedented properties. We also note that the amplitude of the effect discussed here may be optimized by using barriers with greater momentum conservation, such as, for example, epitaxial AlAs.

The authors thank J. Sinova and A. H. MacDonald for useful discussions and V. Hock for sample preparation, and acknowledge financial support from the EC (SPINOSA), the German BMBF (13N8284) and DFG (SFB410), the DARPA SpinS program, and the Grant Agency of the Czech Republic under Grant No. 202/02/0912. One of us (R. G.) thanks the Humbolt Foundation for financial support.

[1] J. S. Moodera, L. R. Kinder, T. M. Wong, and R. Meservey, Phys. Rev. Lett. **74**, 3273 (1995).
[2] Y. Higo, H. Shimizu, and M. Tanaka, J. Appl. Phys. **89**, 6745 (2001).
[3] D. Chiba, F. Matsukura, and H. Ohno, Physica (Amsterdam) **21E**, 966 (2004).
[4] For a discussion of (Ga,Mn)As growth, see, e.g., A. Shen *et al.*, J. Cryst. Growth **175**, 1069 (1997); R. P. Campion *et al.*, J. Cryst. Growth **247**, 42 (2003).
[5] G. M. Schott, G. Schmidt, G. Karczewski, L. W. Molenkamp, R. Jakiela, A. Barcz, and G. Karczewski, Appl. Phys. Lett. **82**, 4678 (2003).
[6] K. W. Edmonds, K. Y. Wang, R. P. Campion, A. C. Neumann, N. R. S. Farley, B. L. Gallagher, and C. T. Foxon, Appl. Phys. Lett. **81**, 4991 (2002).
[7] R. P. Cowburn, S. J. Gray, J. Ferré, J. A. C. Bland, and J. Miltat, J. Appl. Phys. **78**, 7210 (1995).
[8] G. P. Moore, J. Ferré, A. Mougin, M. Moreno, and L. Däwitz, J. Appl. Phys. **94**, 4530 (2003),
[9] H. X. Tang, R. K. Kawakami, D. D. Awschalom, and M. L. Roukes, Phys. Rev. Lett. **90**, 107201 (2003).
[10] D. Hrabovsky, E. Vanelle, A. R. Fert, D. S. Yee, J. P. Redoules, J. Sadowski, J. Kanski, and L. Ilver, Appl. Phys. Lett. **81**, 2806 (2002).
[11] E. C. Stoner and E. P. Wohlfarth, Philos. Trans. R. Soc. London A **240**, 599 (1948).
[12] The full (Ga,Mn)As valence band structure is shown in M. Abolfath, T. Jungwirth, J. Brum, and A. H. MacDonald, Phys. Rev. B **63**, 054418 (2001).
[13] D. Chiba, K. Takamura, F. Matsukura, and H. Ohno, Appl. Phys. Lett. **82**, 3020 (2003).